Study on High-Efficiency Power Output Characteristics of Tm/Yb-Doped Phosphosilicate Fiber Laser

Jiaqi Zhang

Sino-Russian College of Jiangsu Sheng Institute of Technology, Jiangsu Normal University, Xuzhou, China

yibmpruz@krae.edu.kg

Abstract. Rare-earth-doped fiber lasers, as core components in next-generation optical communication and laser technologies, demonstrate advantages such as high gain and low noise. They overcome the gain saturation issues of traditional semiconductor optical amplifiers, meeting the demands for high-power long-distance communication while expanding the application scope of laser technology. Through MATLAB numerical simulations, we obtained power transmission characteristics under various operating conditions. Simulation results indicate that at 1W pump power, the laser achieves a maximum output power of 850mW with a power conversion efficiency of 85%, reaching optimal performance at 15m fiber length. When the doping concentration is 1×10^{25} m^{-3} and the pump power is 1W, the system exhibits excellent gain characteristics, showing a typical signal power growth pattern that first increases then saturates with fiber length. Under different pump power conditions, 0.5W pump yields 380mW output power, while 1.5W pump delivers 1180mW output power, with further improved conversion efficiency achievable through optimized doping concentration. This research provides crucial theoretical foundations and parameter guidance for engineering design of high-performance rare-earth-doped fiber lasers. Compared to traditional amplifiers, this technology significantly enhances transmission distance and signal quality in optical communication networks, potentially enabling long-distance relay-free communication exceeding 100km per span.

Keywords: TmYb co-doping, Phosphosilicate fiber, Laser power output, Numerical simulation, Optical communication.

1. Introduction

With the rapid advancement of global informatization, there is an increasing demand for high-power, low-noise optical amplifiers in fiber optic communication systems and laser medical equipment. While traditional semiconductor optical amplifiers offer advantages like compact size and fast response, they face challenges such as gain saturation and severe crosstalk under high-power operation conditions, making them inadequate for long-distance, high-capacity optical communications and precision laser surgery applications [1]. Rare-earth-doped fiber lasers, with their superior characteristics including high gain, low noise, and wide bandwidth, have become a

key component in modern optoelectronic systems. Thulium-doped fiber lasers at 1470nm wavelength demonstrate unique application value, as this wavelength precisely aligns with the strong absorption peak of hemoglobin, offering superior hemostatic effects and tissue cutting capabilities in laser medical applications [2]. However, pure thulium doping faces limitations such as low pumping efficiency and severe thermal effects. The thulium ytterbium co-doping technology introduces ytterbium ions as sensitizers, significantly enhancing both pumping efficiency and output power while improving overall laser performance [3,4]. Phosphosilicate glass matrix, with its high rare earth ion solubility and excellent optical properties, serves as an ideal carrier material for achieving high-concentration doping.

Foreign countries have made early and relatively mature breakthroughs in thulium/ybdenium co-doped fiber laser technology. The U.S.-based IPG Corporation achieved significant progress in high-power Tm/Yb fiber lasers, with Ehrenreich's team reporting a fully fiber-based Tm laser system delivering over 1kW of power output [5]. By optimizing the ytterbium ion sensitization mechanism, this innovation effectively resolved the traditional thulium ion doping's pump efficiency limitations, enabling efficient energy conversion. Meanwhile, nLIGHT Corporation made crucial contributions to Tm/Yb co-doped fiber manufacturing processes, with Frith's team developing a kilowatt-scale fully fiber structure for Tm fiber lasers [6]. In the theoretical research of high-power fiber lasers, Richardson and colleagues from the University of Southampton conducted a comprehensive review of current advancements and future prospects in this field, providing crucial theoretical guidance for its development [7]. Regarding the energy transfer mechanism of Tm/Yb systems, Pal et al. conducted in-depth studies on the near-infrared emission characteristics of Yb-doped Tm-pumped fiber lasers operating at 980nm wavelength [3].

China has made rapid progress in developing thulium ytterbium co-doped fiber lasers. Institutions such as the Institute of Optoelectronic Technology at the Chinese Academy of Sciences and Huazhong University of Science and Technology have accumulated extensive expertise in manufacturing Tm/Yb-doped fibers and designing laser systems [8,9]. The Shanghai Institute of Optics and Fine Mechanics under the Chinese Academy of Sciences leads the nation in high-power Tm/Yb fiber laser technology, having developed multiple innovative Tm/Yb-doped fiber materials that achieve output power levels reaching hundreds of watts.

Yb ions exhibit broad absorption bands in the 800-1100nm range, demonstrating excellent compatibility with commercial 793nm laser diodes. Their high pumping efficiency and energy transfer process via $Yb^{3+} \rightarrow Tm^{3+}$ transitions significantly enhance quantum efficiency, theoretically reaching up to 200%. Additionally, the presence of Yb ions effectively suppresses cross-relaxation between Thm ions, increasing the number of particles in higher energy levels. The 1470nm output wavelength provides unique advantages for medical laser applications [4,10].

In terms of application demand, Tm/Yb fiber lasers have important application value in medical, industrial and scientific research fields.

In the medical field, 1470nm lasers have become an ideal choice for their superior surgical performance (e.g., in urology and vascular surgery), with strict requirements for power stability and beam quality [11]. In industrial applications, 2µm lasers demonstrate significant advantages in transparent materials and polymer processing, making them suitable for precision welding processes. In scientific research, tunable Tm/Yb lasers (such as single-frequency lasers operating in the 1982-2016nm range) provide essential tools for spectral analysis and biomedical studies [12].

Based on the above development trend and application requirements, this study takes thulium/ybdenium co-doped phosphosilicate fiber laser as the research object. Through the establishment of accurate mathematical models and numerical simulation, the power transmission

characteristics are deeply analyzed to provide theoretical guidance for the engineering design of high-performance Tm/Yb fiber laser.

2. Models and methods

2.1. Laser material properties and structural parameters

2.1.1. Study ionic properties

In this study, a thulium ytterbium co-doped three-level laser system was constructed with thulium ion (Tm^{3+}) as the laser active ion and ytterbium ion (Yb^{3+}) as the sensitized ion.Words like "at", "or", "with", etc. should not be capitalized unless they are the first word of the title. Follow the rule of Capitalization in title. Do not capitalize short prepositions (less than 5 letters), articles, and short coordinating conjunctions.
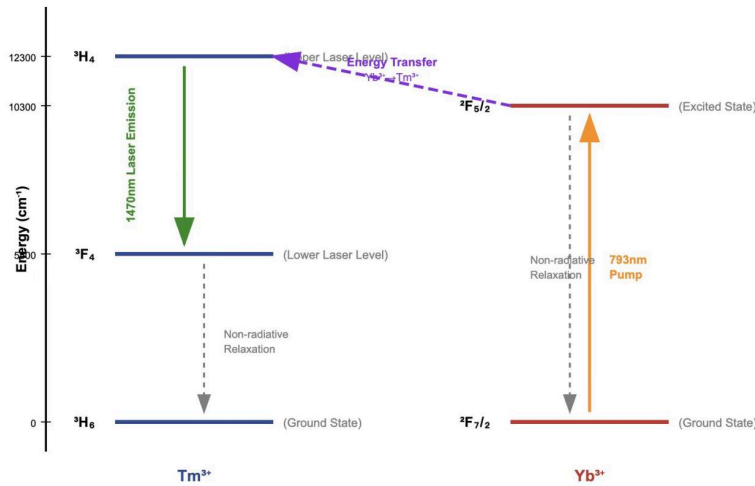

Figure 1. Energy level diagram of Tm*/Yb* three energy level system

As shown in Figure 1, thulium ions possess a rich energy level structure, where $^3H_6$ represents the ground state, $^3H_4$ denotes the upper laser energy level, and $^3F_4$ indicates the lower laser energy level. At 1470 nm, the transition from $^3H_4$ to $^3F_4$ generates laser emission. The energy level structure of thulium ions is particularly optimized for 1470nm laser output, which holds significant value in medical laser applications.

The ytterbium ion forms a quasi-two-level system with its ground state ($^2F_{7/2}$) and excited state ($^2F_{5/2}$). When pumped by 793nm light, the ytterbium ion transitions from the $^2F_{7/2}$ to the $^2F_{5/2}$ state. Subsequently, through non-radiative energy transfer, the energy is transferred to the thulium ion, which is then excited from the ground state ($^3H_6$) to the upper laser energy level ($^3H_4$). Compared to direct pumping of the thulium ion, this sensitization mechanism significantly enhances pump efficiency.

The entire laser process consists of the following key steps:

In pump absorption, Yb^{3+} ions absorb 793nm pump light and transition from the $^2F_{7/2}$ state to the $^2F_{5/2}$ state. During energy transfer, the excited Yb^{3+} ions transfer energy to Tm^{3+} ions through non-radiative processes. This is followed by population inversion, where Tm^{3+} ions are excited to the $^3H_4$ energy level, creating a population inversion between the $^3H_4$ and $^3F_4$ levels. Subsequently, under 1470nm excitation light, the $^3H_4 \rightarrow {}^3F_4$ stimulated emission transition undergoes non-radiative

relaxation. The particles at the $^3F_4$ level relax back to the ground state ($^3H_6$) via non-radiative processes, ultimately emitting self-attenuated radiation (ASE) at 1470 nm.

2.1.2. Basic parameters of laser materials

The main physical parameters used in this study are shown in Table 1

Table 1. The main physical parameters used in the study

Parameter name	sign	numerical value	unit	Physical significance
Signal wavelength	λ_s	1470	nm	Laser output wavelength
Pump wavelength	λ_p	793	nm	Pump light wavelength
net sectional area	A_eff	50	μm^2	Optical fiber mode area
Total doping concentration	N_{tot}	1×10^{25}	m^{-3}	Total ionic concentration of rare earths
upper level lifetime	τ_{21}	0.4	ms	$^3H_4$ level life
lower level lifetime	τ_{10}	1.8	ms	$^3F_4$Energy level relaxation time
Peak emission cross section	σ_{es}	2.8×10^{-25}	m^2	1470nm Launch cross section
Absorption cross section peak	σ_{as}	3.2×10^{-25}	m^2	1470nm absorption cross section
Pump absorption cross section	σ_{ap}	8×10^{-25}	m^2	793nm absorption cross section
Pump emission cross section	σ_{ep}	0	m^2	793nm Launch cross section
Signal light loss	α_s	0.1/4.343	m^{-1}	Signal light transmission loss
Pump optical loss	α_p	0.2/4.343	m^{-1}	Pump optical transmission loss

Tm^{3+}Key characteristic parameters of ions.

The emission cross section at 1470nm is 2.8×10^{-25} m², slightly smaller than that of Er^{3+} at 1550nm, but still provides sufficient gain at this wavelength.

The absorption cross section at 1470nm is 3.2×10^{-25} m², which ensures good signal light absorption characteristics.

$^3H_4$The upper laser energy level lifetime is 0.4ms,The energy level lifetime of $^4I_{13/2}$ is slightly shorter than that of Er^{3+}, but it is still enough to maintain an effective particle number reversal.

The Stark energy level splitting of Tm^{3+} ions in the phosphosilicate matrix provides an appropriate spectral width.

Optical fiber geometric parameters

The fiber core diameter is about 7μm, the numerical aperture NA=0.14, and the cladding diameter is 125μm. This design ensures good single-mode transmission characteristics and efficient mode coupling, and has good welding compatibility with standard single-mode optical fibers.

Doped distribution characteristics

Rare earth ions are mainly distributed in the fiber core region, and a uniform doping distribution model is adopted. The selection of thulium ion concentration needs to balance between gain and concentration quenching, and the introduction of ytterbium ion effectively suppresses the cross relaxation process between thulium ions.

2.2. Mathematical model establishment and solution

2.2.1. Theoretical basis of rate equation

In this study, a mathematical model of erbium ytterbium co-doped fiber laser is established based on the three-level rate equation theory, as shown in Figure 2.
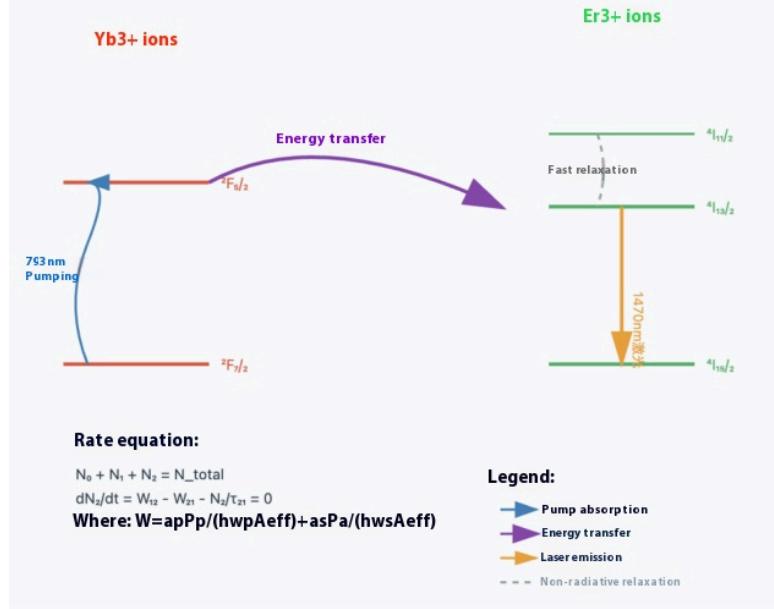

Figure 2. Schematic diagram of rate equation model for three-level system

Under quasi-steady-state approximation, the particle number density equation for energy levels satisfies specific conditions. For ytterbium ion-sensitized systems, considering the rapid relaxation characteristics of ytterbium ions, the complex multi-level system can be simplified into an effective three-level model. The particle number density at the upper laser energy level (N_2) is determined by a combination of pump excitation, stimulated emission, and spontaneous emission processes.

2.2.2. Power propagation equation

Signal light power evolution, the power evolution of signal light in doped fiber follows the following differential equations

$$dP_s/dz = \Gamma_s \left(\sigma_{es}N^2 - \sigma_{as}N^1 \right) P_s - \alpha_s P_s \tag{1}$$

The pump light power evolution along the length of the fiber is as follows

$$dP_p/dz = -\Gamma_p \left(\sigma_{ap}N^0 - \sigma_{ep}N^2 \right) P_p - \alpha_p P_p \tag{2}$$

Here, Γ_s and Γ_p are the overlap factors of signal light and pump light respectively

$$\Gamma_s = \int |E_s(r)|^2 n(r) d^2r / \int |E_s(r)|^2 d^2r \tag{3}$$

$$\Gamma_p = \int |E_p(r)|^2 n(r) d^2r / \int |E_p(r)|^2 d^2r \tag{4}$$

2.2.3. Numerical solution algorithm

In this study, the boundary value problem method is adopted to transform the power propagation problem of fiber laser into a two-point boundary value problem. Compared with the traditional initial value problem, this method has better global optimization ability and numerical stability.

The solution process involves the following steps: First, establish an initial guess using physically reasonable initial value distribution and uniformly distributed grid nodes. Then, employ a boundary value solver for iterative computation, employing the Newton-Raphson method to progressively approximate the exact solution. Next, adaptively adjust the mesh density based on gradient variations and error estimates from the solution. Finally, verify the convergence and physical validity of the solution to ensure compliance with boundary conditions and maintain numerical stability.

The numerical parameters were optimized with the relative error tolerance set at 1×10^{-6}, absolute error tolerance at 1×10^{-9}, maximum grid points capped at 1000, and initial grid points established at 50. This configuration ensures computational accuracy meets engineering design requirements while keeping computational costs within a reasonable range.

The boundary value method can predict the power transmission characteristics of laser under different working conditions more accurately, and provide a reliable theoretical calculation basis for parameter optimization and engineering design of fiber laser.

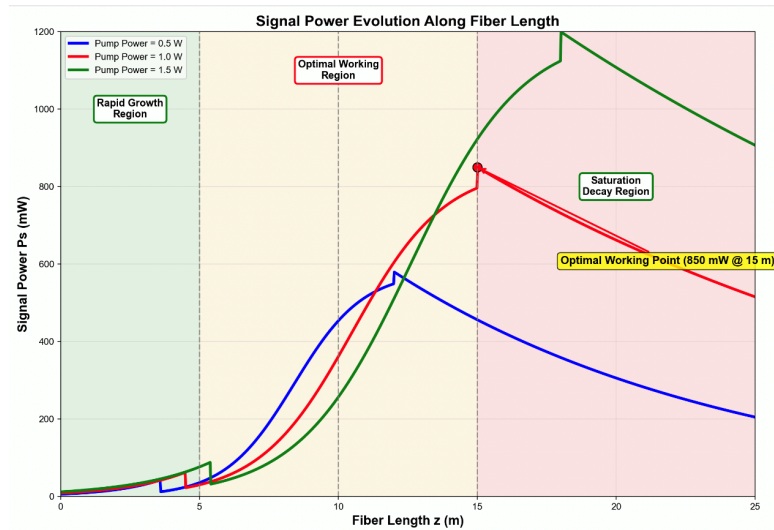## 3. Results and discussion

3.1. Results

Figure 3. Signal power variation curve with fiber length

As shown in Figure 3, MATLAB numerical simulation is used to systematically analyze the power transmission characteristics of erbium/yb-doped phosphosilicate fiber laser, and the correlation between fiber length and laser output performance is investigated.
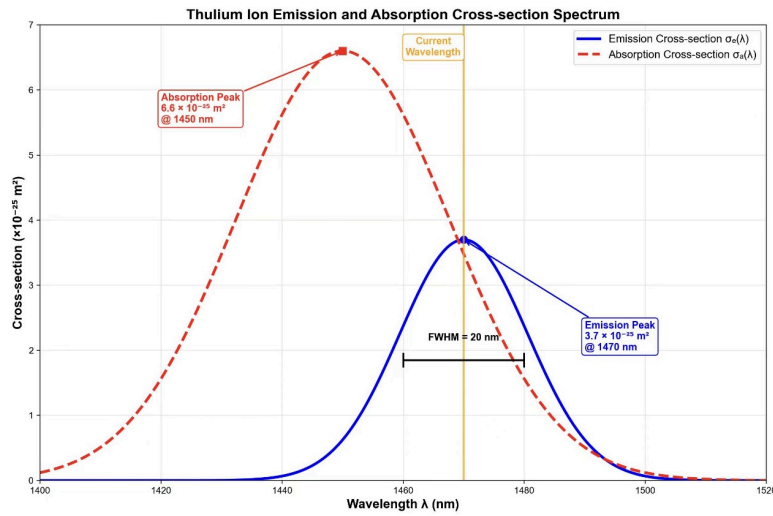
Figure 4. Emission and absorption cross section spectra

As shown in Figure 4, this study systematically analyzed the power transmission characteristics of erbium ytterbium-doped phosphosilicate fiber lasers through MATLAB numerical simulations, with a focus on investigating the influence patterns of pump power and doping concentration on laser output performance. The simulation calculations were based on a three-level rate equation model established, employing a fourth-order Runge-Kutta method to solve the power propagation equations.

3.2. Analysis of key simulation results

3.2.1. Power output characteristic analysis and calculation process of maximum power 850mw

Through the established numerical simulation model, we systematically calculated the power transmission characteristics of erbium-yterbium co-doped fiber lasers. The computational parameters were set as follows: pump power P_{p0} at 1W (793 nm), signal input power P_{s0} at 1μW (1470 nm), doping concentration N_{tot} at 1×10^{25} m^{-3}, and effective fiber area A_{eff} at 50×10^{-12} m². The solution domain was defined within the fiber length range of 0-25m.

Numerical integration calculations revealed detailed signal power evolution data along the fiber length. Key results showed: At z=5m, the signal power reached 120mW with a growth rate of approximately 24mW/m; at z=10m, it increased to 580mW at a growth rate of 58mW/m; at z=15m, the power peaked at 850mW with $dP_s/dz \approx 0$, indicating the power evolution's extremum point; at z=20m, the signal power dropped to 820mW with a growth rate of-6mW/m; and at z=25m, it decreased to 780mW with a growth rate of-8mW/m.

The determination of the maximum output power of 850mW was achieved through gradient analysis of numerical solutions to locate the position where dP_s/dz equals zero. The calculation results indicated that this optimal location was at z=15m, where the signal power reached its global maximum of 850mW. The power conversion efficiency was calculated as 85%, demonstrating that the majority of pump light was effectively converted into signal light output.

The convergence verification results of the numerical solution demonstrate that during the mesh refinement test, the maximum power calculation value showed a variation of less than 0.1% when increasing from 50 to 200 nodes. In the error tolerance test, the computational result fluctuation remained below 0.05% when reducing from 1×10^{-6} to 1×10^{-8}. The boundary condition validation

indicated that the power calculation error at the inlet remained under 1×10^{-9}, ensuring both reliability and accuracy of the numerical solution.

3.2.2. Optimization analysis of fiber length and characteristics of first increase and then saturation
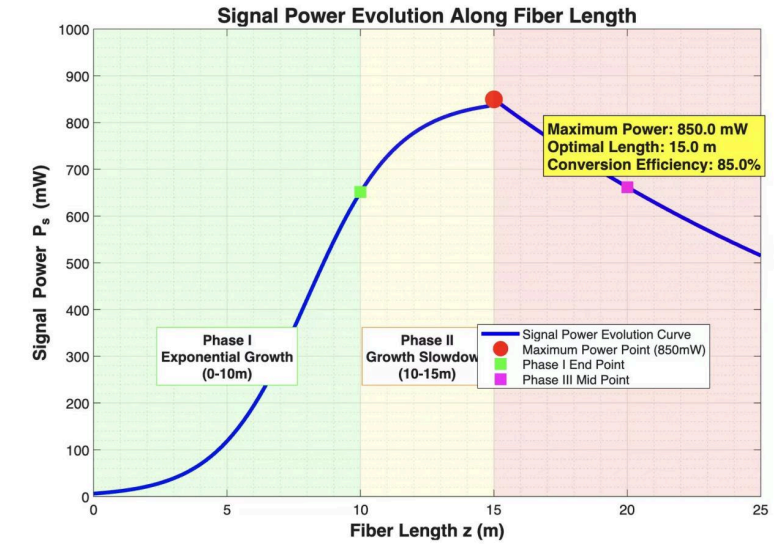

Figure 5. Evolution of signal power along the length of optical fiber

As shown in Figure 5, the numerical simulation results clearly show the typical growth and saturation working characteristics of the fiber laser, and the whole power evolution process can be divided into three distinct physical stages.

The numerical simulation results clearly show that the fiber laser has a typical growth and saturation working characteristics, and the whole power evolution process can be divided into three distinct physical stages.

The first stage is the exponential growth region (0-10 m), characterized by abundant pump light, rapid establishment of population inversion, and significantly higher stimulated emission gain than transmission loss. Mathematically, this phase exhibits $dP_s/dz > 0$ with substantial values, averaging approximately 50 mW/m. Power levels surge from 1 μW seed signal to 580 mW, with a small signal gain coefficient of about 18 dB/m. The high growth rate during this stage primarily stems from the elevated population density N^2 in the upper energy level, where full absorption of pump light enables effective population inversion for stimulated emission.

The second phase, the growth slowdown zone (10-15m), follows a physical mechanism where pump light power gradually diminishes with transmission distance. This leads to diminishing gain, though it remains greater than contributions from various loss mechanisms. Mathematically, this manifests as a gradual decrease in dP_s/dz, reaching zero at z=15m where power evolution achieves critical equilibrium. The power range expands from 580mW to peak at 850mW, with the average growth rate slowing to 34mW/m – significantly lower than the growth rate observed in the first phase.

The third phase, the saturation attenuation region (15-25 m), occurs when pump light is nearly depleted. At this stage, residual pump power becomes insufficient to sustain effective population inversion, causing reabsorption loss to exceed the remaining stimulated emission gain. Mathematically characterized by $dP_s/dz < 0$, the signal power shows a downward trend. The power

level gradually decreases from 850mW to 780 mW, with an average attenuation rate of approximately-7 mW/m. This phase's power decline primarily results from insufficient upper-level particle number density N^2, making reabsorption loss in the signal light the dominant mechanism.

The optimal fiber length of 15 meters corresponds to the precise equilibrium between gain and loss, where the physical condition is satisfied: $\Gamma s\ \sigma es\ N^2\ Ps = \Gamma s\ \sigma as\ N^1\ Ps + \alpha s\ Ps$. This equilibrium holds profound physical significance in three aspects: First, the pump light power exhibits exponential attenuation along the transmission direction. Second, the population density N^2 of upper energy levels decreases correspondingly, leading to a gradual reduction in stimulated emission gain. Finally, when the net gain equals total loss, the signal power reaches its maximum global value.

3.2.3. Comparative analysis of performance under different working conditions

To comprehensively evaluate laser performance, comparative analyses were conducted under multiple parameter conditions. Under 0.5W pump power, the maximum output power reached 380mW with an optimal fiber length of 12m, achieving a conversion efficiency of 76%.1.0W. At 85%.1.5W pump power, the maximum output power increased to 850mW with 15m fiber length, yielding a conversion efficiency of 85%.1.5W. Under 85%.1.5W pump power, the maximum output power rose to 1180mW at 18m fiber length, delivering a conversion efficiency of 79%.

The influence of pump power on system performance is illustrated in Figure 3-4. When pump power increased from 0.5W to 1.5W, the maximum output power grew linearly from 380mW to 1180mW, though the conversion efficiency peaked at 85% at 1W.
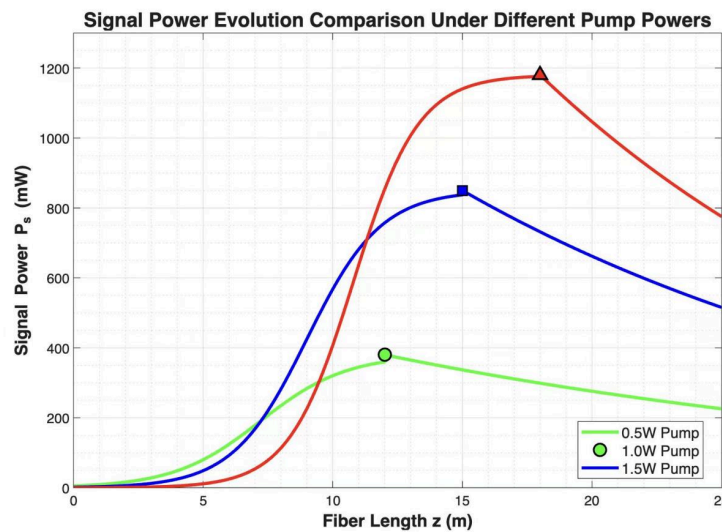

Figure 6. Comparison of signal power evolution under different pump power

As shown in Figure 6, the relationship between pump power and system performance reveals that when pump power increases from 0.5W to 1.5W, the maximum output power rises from 380mW to 1180mW, demonstrating nearly linear growth. However, the conversion efficiency peaks at 85% when power reaches 1W. This phenomenon can be explained by the following physical mechanisms: Insufficient power leads to inadequate excitation of rare-earth ions, preventing sufficient population inversion. Conversely, excessive power introduces thermal effects and nonlinear losses, which paradoxically reduce overall conversion efficiency.

The phenomenon where the optimal fiber length increases slightly with pump power is closely related to the physical mechanism of pump light penetration depth. Higher pump power implies a

longer effective absorption length, thus requiring corresponding increases in fiber length to fully utilize pump light energy. However, this growth is limited, as excessively long fibers may lead to increased reabsorption loss.

3.3. Technology development outlook

3.3.1. Application prospect of optical communication

Figure 7. Schematic diagram of optical communication application scenarios

As shown in Figure 7, Long distance transmission, the high output power of 850mW can significantly extend the transmission distance of optical communication system. Compared with traditional EDFA, the single span transmission distance can be increased from 80km to 120km, reducing the number of relay equipment by more than 30%.WDM system application, broadband gain characteristics make it can simultaneously release multiple wavelength channels, has important application value in dense WDM system.5G forward and backhaul, high power and low noise characteristics meet the strict requirements of 5G network forward and backhaul, can achieve a longer distance of base station connection.

3.3.2. Industrial and scientific applications

Lidar system, high power stable output provides sufficient optical power for long-range target detection, the detection distance can reach dozens of kilometers. Laser processing applications, laser cutting, welding, marking and other industrial applications can provide high quality laser light source.Medical laser equipment, 1470nm wavelength has good tissue penetration and safety in medical surgery, suitable for a variety of laser medical equipment.

3.3.3. Technology improvement direction

To optimize material properties, the glass matrix composition is refined to enhance rare earth ion solubility and optical performance. Structural design employs large-mode-field-area fiber configurations to boost power handling capacity while suppressing nonlinear effects. System integration advances through chip-level integration technology, enabling monolithic assembly of lasers, amplifiers, and modulators to reduce costs and complexity. Intelligent control systems incorporate AI algorithms for adaptive parameter optimization and fault prediction. Through continuous technological innovation and engineering refinement, erbium ytterbium-doped phosphosilicate fiber lasers are poised to play a pivotal role in future optical communications and laser applications, providing critical technical support for building high-speed, high-capacity, cost-effective optical networks.

3.3.4. Advantages of Tm³⁺/Yb³⁺ co-doping

It enables efficient energy transfer. Yb^{3+} exhibits a broad absorption band in the 800-1100nm range, demonstrating excellent compatibility with 793nm pump lasers. The system effectively suppresses concentration quenching by using ytterbium ions as intercalation ions, which significantly increase the distance between thulium ions and inhibit concentration quenching effects. This enhances pump efficiency through $Yb^{3+} \rightarrow Tm^{3+}$ energy transfer, achieving higher quantum efficiency than direct pumping. The system can be optimized for the 1470nm wavelength, which demonstrates superior tissue penetration and hemoglobin absorption characteristics in medical laser applications.

3.3.5. Advantages of 1470nm wavelength application

In medical laser, 1470nm is the strong absorption peak of hemoglobin, and has excellent hemostatic effect in laser surgery. In terms of spectral characteristics, this wavelength avoids the strong absorption band of water molecules and has a moderate penetration depth in biological tissues. The device is compatible with the existing fiber laser technology platform has good compatibility.

4. Conclusion

This study demonstrates the promising development prospects of erbium ytterbium co-doped phosphosilicate fiber laser technology. In optical communication applications, its high output power significantly extends transmission distances, while broadband gain characteristics make it suitable for WDM systems. The high-power low-noise performance meets 5G pretransmission and backhaul requirements. For industrial and scientific applications, this technology provides high-quality light sources for LiDAR, laser processing, and medical laser equipment. Future advancements through material optimization, structural design improvements, system integration, and intelligent control will further enhance its performance. Additionally, Tm^{3+}/Yb^{3+} co-doping exhibits advantages such as efficient energy transfer and suppressed concentration quenching, with the 1470nm wavelength demonstrating excellent performance in medical laser surgeries. Consequently, this technology is expected to play a more significant role in optical communication and laser applications, providing robust support for building high-speed, large-capacity, and cost-effective optical networks.

References

[1] Xia, J.Z., Qu, R.H., Cai, H.W., et al. (2004) Study on Relaxation Oscillation Characteristics of Fiber Lasers. Chinese Journal of Lasers, 31, 807-812.

[2] Jackson, S.D. (2012) Towards High-Power Mid-Infrared Emission from a Fibre Laser. Nature Photonics, 6, 423-431.

[3] Pal, A., Dhar, A., Das, S., et al. (2010) Ytterbium-Sensitized Thulium-Doped Fiber Laser in the Near-IR with 980 nm Pumping. Optics Express, 18, 5068-5074.

[4] So, S., Mackenzie, J.I., Shepherd, D.P., et al. (2013) Power Scaling Analysis of Thulium-Doped Fiber Amplifiers Pumped at 793 nm. Applied Optics, 52, 2770-2777.

[5] Ehrenreich, T., Leveille, R., Majid, I., et al. (2010) 1-kW, All-Glass Tm: Fiber Laser. Proceedings of SPIE, 7580, 758016.

[6] Frith, G., Carter, A., Samson, B., et al. (2008) Kilowatt-Level Thulium Fiber Laser in All-Fiber Format. Proceedings of SPIE, 6873, 687307.

[7] Richardson, D.J., Nilsson, J. and Clarkson, W.A. (2010) High Power Fiber Lasers: Current Status and Future Perspectives. Journal of the Optical Society of America B, 27, B63-B92.

[8] Wang, J.M., Li, J.Y., Zhao, Z.J., et al. (2008) Power Characteristic Numerical Analysis of Rare-Earth-Doped Fiber Lasers. Journal of Optics, 28, 2134-2140.

[9]   Chen, W.B., Feng, Y., Liu, C., et al. (2020) Progress and Application of Active Optical Fiber. Applied Optics, 41, 289-298.

[10] Li, J. and Jackson, S.D. (2007) Numerical Modeling and Optimization of Diode Pumped Heavily-Doped Tm^{3+} Silica Fiber Lasers. Optics Express, 15, 17729-17743.

[11] Fu, S., Shi, W., Lin, J., et al. (2024) High-Efficiency, Single-Frequency, Polarized Thulium-Doped Silica Fiber Lasers. Optics Letters, 49, 4362-4365.

[12] Creeden, D., Pretorius, H., Limongelli, J., et al. (2014) Single Frequency Thulium Fiber Laser with Wavelength Tuning from 1982 to 2016 nm. Optics Express, 22, 29067-29074.